Icarus 225 (2013) 949–959

Contents lists available at SciVerse ScienceDirect

Icarus

journal homepage: www.elsevier.com/locate/icarus

Response timescales for martian ice masses and implications for ice flow on Mars

Michelle R. Koutnik [a,b,*], Edwin D. Waddington [b], Dale P. Winebrenner [b,c], Asmin V. Pathare [d]

[a] Centre for Ice and Climate, Niels Bohr Institute, University of Copenhagen, Juliane Maries Vej 30, 2100 Copenhagen, Denmark
[b] Department of Earth and Space Sciences, Box 351310, University of Washington, Seattle, WA 98195, United States
[c] Applied Physics Laboratory, Box 355640, University of Washington, Seattle, WA 98195, United States
[d] Planetary Science Institute, 1700 E. Ft. Lowell, Suite 106, Tucson, AZ 85719, United States

ARTICLE INFO

Article history:
Available online 17 October 2012

Keywords:
Mars, Surface
Mars, Polar caps
Mars, Climate

ABSTRACT

On Earth and on Mars, ice masses experience changes in precipitation, temperature, and radiation. In a new climate state, flowing ice masses will adjust in length and in thickness, and this response toward a new steady state has a characteristic timescale. However, a flowing ice mass has a predictable shape, which is a function of ice temperature, ice rheology, and surface mass-exchange rate. In addition, the time for surface-shape adjustment is shorter than the characteristic time for significant deformation or displacement of internal layers within a flowing ice mass; as a result, surface topography is more diagnostic of flow than are internal-layer shapes. Because the shape of Gemina Lingula, North Polar Layered Deposits indicates that it flowed at some time in the past, we use its current topography to infer characteristics of those past ice conditions, or past climate conditions, in which ice-flow rates were more significant than today. A plausible range of near-basal ice temperatures and ice-flow enhancement factors can generate the characteristic geometry of an ice mass that has been shaped by flow over reasonable volume-response timescales. All plausible ice-flow scenarios require conditions that are different from present-day Mars, if the basal layers are pure ice.

1. Introduction

On Earth, a valuable archive of past-climate information can be accessed directly by drilling an ice core. However, it is important to recognize that ice-surface topography and the shapes of internal layers are also informative about terrestrial ice-sheet and climate histories. The large polar ice masses of Mars, the Polar Layered Deposits (PLD), probably play a similar role on Mars, by archiving information about past martian climate. Although a martian ice core has not yet been recovered, topography, radar observations, and imagery of the martian PLD are available, and these data can provide information about the ice and climate histories on Mars.

On Earth, radar data reveal internal layers in glaciers and ice sheets, and those data are an integral part of understanding the history of terrestrial ice masses because they provide distinct spatial information. Internal layers are past ice-sheet surfaces that have been subsequently buried by accumulation and modified by ice flow; internal layers are considered to be surfaces of constant age (isochrones). Because we know that terrestrial ice masses flow, we can use physically based flow models together with the radar-observed layers to understand terrestrial climate and ice-flow histories (e.g. Vaughan et al., 1999; Hindmarsh et al., 2006; Waddington et al., 2007; Leysinger Vieli et al., 2011). On Mars, radar data also reveal internal layers in polar ice masses. Using martian ice-surface topography and internal layers together in order to understand the history of martian ice masses is an important goal. However, the Mars research community has yet to reach a consensus as to whether the PLD ever flowed.

Ice flow is a dynamic response to gravitational shear forces acting on an ice mass due to the shape of its sloping free surface. That free surface is in turn shaped by the flow, and therefore the shape of the ice surface is indicative of whether or not it flowed. The ice-surface topography is more diagnostic of the ice-flow history than the shapes of internal layers, which can be created in many different ways, with or without flow. As a result of this non-uniqueness, internal layers contain little information about the presence or absence of flow, and internal layers alone cannot be used to test the hypothesis that the ice has flowed. Before their shapes can be interpreted in terms of surface accumulation and ablation (mass-exchange) patterns, it must be decided *a priori* if there was or was not flow that influenced the layer shapes.

Using a kinematic flow model that did not test the dynamic shape of the ice surface of Gemina Lingula, Karlsson et al. (2011) suggested that internal-layer patterns there indicated that the ice had not experienced flow if one particular and idealized surface mass-exchange pattern was used. However, they also mentioned that different mass-exchange histories could improve their flow-model fits to Gemina Lingula radar-observed layers. We emphasize

* Corresponding author at: Department of Earth and Space Sciences, Box 351310, University of Washington, Seattle, WA 98195, United States.
E-mail address: mkoutnik@uw.edu (M.R. Koutnik).

0019-1035/$ - see front matter © 2012 Elsevier Inc. All rights reserved.
http://dx.doi.org/10.1016/j.icarus.2012.09.031

that since the mass-exchange history is unknown, then a PLD history with at least one episode of significant ice flow cannot be ruled out.

The surface shape is relatively independent of spatial details of the pattern of accumulation and ablation (e.g. Cuffey and Paterson, 2010, p. 385). Koutnik et al. (2009), Fig. 5 showed that, in the presence of flow, different accumulation and ablation patterns could create very similar ice-surface profiles, yet lead to very different internal-layer shapes. Winebrenner et al. (2008) used a simple ice-flow model to show that the shape of the inter-trough Mars Orbiter Laser Altimeter (MOLA; e.g. Zuber et al., 1998) topography along flowbands across Gemina Lingula, North PLD (NPLD) provides strong evidence for flow there at some point in the past. Their inferred Gemina Lingula geometry and surface mass-exchange pattern generated excellent reconstructions of the topography between troughs, indicating that at some time in the past, mass exchange at the surface was approximately balanced by ice flow, i.e. the ice mass was in, or near, steady state, and the troughs dissecting the present-day surface were filled with ice. This era of ice flow may have lasted long enough for the ice surface to approach steady state, but not necessarily long enough for the internal layers to approach steady state; this is discussed further in Section 2.4.

It is not the motivation of this paper to directly address the question whether ice flow on Mars significantly shaped martian ice masses; for example, see Winebrenner et al. (2008, 2011, 2012). However, this work is an important extension of Winebrenner et al. (2008) because radar-based arguments against ice flow (e.g. Holt et al., 2011) and specific tests of flow hypotheses (e.g. Karlsson et al., 2011) are by their nature inconclusive. In this paper we calculate combinations of ice temperature and ice-flow enhancement that will produce the shape of Gemina Lingula reconstructed by Winebrenner et al. (2008). We also calculate the amount of time it takes for ice flow to shape the ice surface for these combinations of conditions; the range of plausible timescales can be used to constrain the range of ice temperature and ice-flow enhancement. We emphasize these points and new findings:

(1) Internal-layer shapes alone cannot be used to address the question of ice-flow history on Mars; this is not a well-posed problem. As shown in Koutnik et al. (2009), internal-layer shapes can be informative about the surface-mass-exchange history, whereas, as shown by Winebrenner et al. (2008), the ice-surface topography can be informative about the existence of a ice flow during some era.
(2) Any episode of ice flow required conditions different than present-day Mars. At present it is too cold on Mars for ice flow to significantly shape Gemina Lingula. For flow to shape the ice surface in a realistic amount of time, the ice had to be warmer and the ice flow likely was enhanced. Our work motivates separate studies of ice rheology and possible enhanced flow on Mars when the ice includes chemical impurities known to occur in martian soils and dust (e.g. perchlorates in the laboratory work of Lenferink et al. (2012)).
(3) After a change in surface mass exchange or in boundary forcing, the adjustment time to approach a new steady state for the ice surface is faster than the adjustment time for internal layers (e.g. Jóhannesson et al., 1989; Hindmarsh, 1996). With large swings in martian climate, flow could have been episodic, and the ice surface could easily have approached a steady-state shape while the internal layers did not. Consequently, surface topography is generally more diagnostic of episodes of flow than are internal-layer shapes.
(4) While there is debate about the ice-flow history of Gemina Lingula and the PLD (e.g. mentioned in review by Byrne (2009)), there is agreement that the shape of other features on Mars indicates that they flowed in the past. For example, Lobate Debris Aprons (e.g. Colaprete and Jakosky, 1998; Mangold and Allemand, 2001; Holt et al., 2008; Plaut et al., 2009; Parsons et al., 2011) and ice-filled craters (e.g. Armstrong et al., 2005; Banks and Pelletier, 2008; Shean, 2010) are pervasive, and ancient glaciers and ice sheets (e.g. Head et al., 2005; Shean et al., 2005; Fastook et al., 2012; Dickson et al., 2012) were likely extensive. These observations further motivate the specific study we present here, and we suggest how our results may be extended to other ice masses on Mars.

2. Background

2.1. Characteristics of a flowing ice mass

A flowing ice mass has a predictable surface shape because of the relationship between driving stress and ice rheology, and this shape can be characterized by the maximum thickness and the length (half width of a radial feature). Ng et al. (2010), Table 1 inventoried terrestrial ice masses, and for the ice caps and ice sheets in their inventory they reported that the ice thicknesses vary between 345 and 3200 m and the lengths vary between 2 km (small ice caps) and 1160 km (in East Antarctica). On Earth, the smaller ice masses, especially valley glaciers, are influenced by bed topography and slope (e.g. Ng et al., 2010, Fig. 4) and for this reason we do not compare small terrestrial glaciers here. On Mars, the smaller ice masses may also be influenced by bedrock topography and slope but the bedrock beneath larger ice masses on Mars appears to be relatively flat. The NPLD bedrock is particularly flat (e.g. Phillips et al., 2008). As terrestrial ice masses get bigger in size they become more quasi-parabolic in shape because the bed topography has less influence. This may be true for some martian ice masses, but this may not be true for present-day Planum Boreum, NPLD and Planum Australe, South PLD (SPLD). While portions of the present-day PLD topography may be consistent with past ice flow (e.g. Zwally et al., 2000), Winebrenner et al. (2008) found that erosion and/or deposition appears to have significantly modified the overall surface of the PLD with the exception of Gemina Lingula, NPLD.

Fig. 1 compares thickness H and length L for terrestrial ice caps and ice sheets (data from Ng et al. (2010), Table 1) with Planum Boreum and Planum Australe (e.g. Zuber et al., 1998), Gemina Lingula (Winebrenner et al., 2008), and Lobate Debris Aprons (LDA; e.g. Mangold and Allemand, 2001, Table 1) on Mars. Fig. 1a shows that the thicknesses and lengths characteristic of martian ice masses under Mars gravity g_{Mars} are not obviously different from terrestrial ice masses under Earth gravity g_{Earth}. Fig. 1b accounts for lower martian gravity by using a plastic-flow relationship to scale the martian thicknesses by $\sqrt{g_{\text{Mars}}/g_{\text{Earth}}}$. Martian ice masses under Earth gravity would be thinner to achieve the same length, and with this gravitational scaling the martian ice masses even more closely follow the thickness-to-length relationship observed on Earth.

Table 1
Parameter values for a characteristic flowband on Gemina Lingula, NPLD.

Inferred parameter	Value
Maximum ice thickness, H	1900 m
Flowband length, L	317 km
Equilibrium line position, R	0.66L
Ratio of accumulation to ablation, c/a	0.56
Ice-flow law exponent, n	3

These values were inferred by Winebrenner et al. (2008) for one characteristic flowband across Gemina Lingula, NPLD.

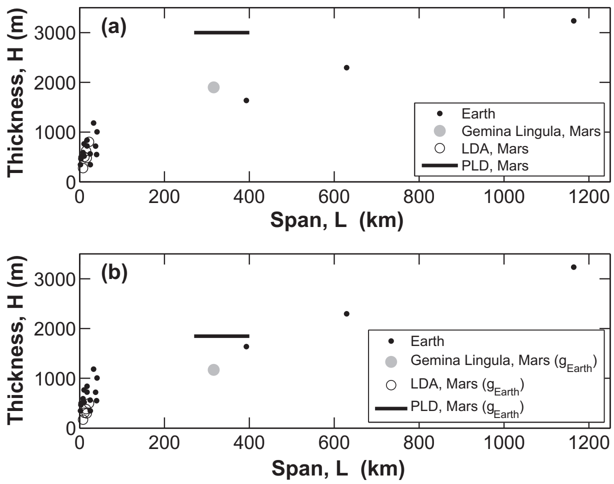

Fig. 1. Maximum ice thickness and length for terrestrial ice masses (from Ng et al. (2010); black dots) compared to Gemina Lingula, NPLD (gray dot), Lobate Debris Aprons (LDA) on Mars (Mangold and Allemand, 2001; open circles), and the range of values for PLD on Mars (Zuber et al., 1998). (a) Values on all length scales, with East Antarctica the largest ice mass on Earth. (b) Thickness and length of martian ice masses fall in line with terrestrial ice masses when martian values are gravitationally scaled to terrestrial gravity g_{Earth} to account for lower gravity on Mars.

Therefore, the ratio of thickness H to span L (H/L) can be used as a crude diagnostic of flow. The higher values of H/L are for smaller ice masses, and the terrestrial ice masses shown here that are thicker than 500 m all have $H/L < 0.08$. Terrestrial ice caps and ice sheets range from $H/L \sim 0.0028$ to 0.1725 with Greenland having $H/L \sim 0.0037$. Gemina Lingula under Mars gravity has $H/L = 0.006$, but the value of H/L for Gemina Lingula when scaled to Earth gravity $\sim$0.0037. Compared to ice masses, various types of sand dunes have a wide variety of shapes but in general they all have steeper slopes and therefore a higher thickness to length ratio. Sand dunes on Earth typically have $H/L \sim 0.1$ (e.g. Lancaster, 1995, p. 73), and Mars' dunes have a similar ratio (e.g. Bourke et al., 2006). While most sand dunes are much smaller features than the PLD, adjacent to Planum Boreum, NPLD there is the likely sand-rich Olympia Planum. One cross section of this feature (Byrne, 2009, Fig. 1) has a thickness $H \sim 310$ m and length $L \sim 250$ km, i.e. $H/L = 0.124$, which falls outside the expected range for a flowing ice mass. While it is only one point, Gemina Lingula fits the pattern well.

2.2. Ice-surface topography

No ice mass is strictly in steady state. However, terrestrial ice masses often approximate steady state because the surface shape is determined by mass conservation (e.g. Cuffey and Paterson, 2010, p. 390):

$$\frac{\partial h}{\partial t} = \dot{b} - \frac{\partial q}{\partial x} \tag{1}$$

where h is ice thickness, $\dot{b}$ is surface mass-exchange rate (accumulation and ablation), and q is ice flux. Terrestrial ice masses usually exhibit a rough balance between flux divergence and mass-exchange rate, so that temporal variations in ice thickness are small. There are cases where mass exchange dominates compared to flow; these ice masses are stagnant (e.g. Cuffey and Paterson, 2010, p. 390; Paterson, 1969; see Meighen Ice Cap example in Fig. 2). There are also cases where flow dominates compared to mass exchange; these ice masses are surging.

Fig. 2 shows steady-state ice-surface profiles for Gemina Lingula reconstructed by Winebrenner et al. (2008) together with two profiles generated using a model with ice dynamics identical to the model in Winebrenner et al. (2008) but with different surface mass-exchange patterns driving those dynamics: (1) a mass-exchange pattern that has a larger ablation zone (normalized equilibrium-line position $R = 0.1$) and (2) a mass-exchange pattern that has a smaller ablation zone ($R = 0.9$) relative to the total flowband length. The equilibrium-line position R is where the mass-exchange pattern transitions from accumulation to ablation; $R = 0.1$ has accumulation over 10% of the ice mass and ablation over 90% of the ice mass. The Gemina Lingula profiles that were reconstructed by an ice-flow model (Winebrenner et al., 2008) all have a similar shape, regardless of details of the mass-exchange pattern. In comparison, the profile across the stagnant Meighen Ice Cap in Arctic Canada (e.g. Paterson, 1969) is very different from a flowing ice mass because the mass-exchange pattern dominates the surface shape.

2.3. Ice flow and ice-surface topography

The simplest flow law for ice is to assume perfect plasticity so that the basal shear stress everywhere is equal to the yield stress. However, this approximation can be improved by using an empirically derived flow law for ice. A creep relationship between shear strain rate and shear stress for ice was determined from laboratory experiments (e.g. Glen, 1955) and generalized by Nye (1957):

$$\dot{\varepsilon}_{xz} = EA(T(x,z))\tau_{xz}^{n} \tag{2}$$

where $\dot{\varepsilon}_{xz} = \frac{1}{2}\frac{\partial u}{\partial x}$ is the simple-shear strain rate along a horizontal plane, E is the dimensionless ice-flow enhancement factor (see Section 4.3), $T(x, z)$ is the ice temperature, τ_{xz} is the shear stress along a horizontal plane. Based on laboratory experiments n typically has a value of 3 for dislocation creep, and $A(T(x, z))$ is the temperature-dependent softness parameter for ice I_h (in $\mathrm{Pa}^{-n}\,\mathrm{yr}^{-1}$; e.g. Cuffey and Paterson, 2010, pp. 55–64). Softness follows an Arrhenius relationship:

$$A(T) = A_0 \exp\left(-Q/R_0T\right) \tag{3}$$

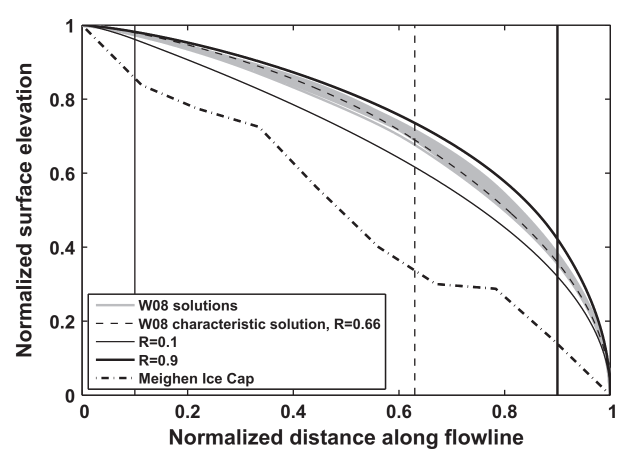

Fig. 2. Comparison of the characteristic flowband solution used in this study (black dashed line) from Winebrenner et al. (2008; W08) to normalized surface profiles from 8 different solutions (gray lines) from Winebrenner et al. (2008), to surfaces generated with very different mass-exchange patterns (black solid lines), and to the profile from stagnant Meighen Ice Cap, Arctic Canada (dashed-dot line). The characteristic solution used here has a normalized equilibrium line position $R = 0.66$ along the length of the flowband. Two extremes of this mass-exchange pattern are $R = 0.1$ (thin black line) with a larger ablation zone and $R = 0.9$ (thick black line) with a smaller ablation zone. The equilibrium-line positions are shown with vertical lines. The differences in the surfaces from different mass-exchange patterns are small compared to the difference between these surfaces and the stagnant Meighen Ice Cap.

where A_0 is the temperature-independent ice-softness parameter ($A_0 = 4.1335 \times 10^{-4}$ kPa^{-3} s^{-1} for a flow-law exponent $n = 3$; calculated from values given by Paterson (1994, p. 97)), Q is the activation energy for creep ($Q \sim 60$ kJ mol^{-1} for temperatures below -10 °C), and R_0 is the universal gas constant ($R_0 = 8.314$ J mol^{-1} K^{-1}). The ice-flow enhancement factor E can account for variations in the physical properties of ice (e.g. chemical impurities, dust, or crystal orientation fabric) that enhance or retard the deformation rate, and terrestrial enhancement factors may be as high as 100 (e.g. Cuffey and Paterson, 2010, p. 315; Section 4.3).

Near-basal ice temperature can be simply related to the surface temperature using Fourier's law of heat conduction in 1-D:

$$q = -k(T)\frac{\partial T}{\partial z} \tag{4}$$

where q is the heat flux (in W m^{-2}), k is the conductivity (in W m^{-1} K^{-1}), T is the temperature (in K), and z is the depth (in m). The conductivity K is a function of temperature (e.g. Cuffey and Paterson, 2010, p. 400; illustrated in Fig. 4a):

$$k(T) = 9.828\exp(-5.7 \times 10^{-3}T) \tag{5}$$

Fig. 3 shows the surface temperature required to produce near-basal temperatures from 200 to 270 K for different values of heat flux. We compare surface temperatures associated with heat fluxes of 10–100 mW m^{-2} (where a value of 20–30 mW m^{-2} is often assumed on Mars, e.g. Clifford, 1993; Grott et al., 2007), and we use a total ice thickness of 1900 m. For example, if the heat flux is 20 mW m^{-2} and the near-basal ice temperature is 230 K, then the surface temperature would be ~215 K.

In the Paterson (1972) model for ice-surface topography, the maximum ice thickness H is related to length L through,

$$H^{2+(2/n)} = \mathbf{K}L^{1+(1/n)} \tag{6}$$

where $\mathbf{K}$ is given by

$$\mathbf{K} = \frac{2(n+2)^{1/n}}{\rho g}\left(\frac{c}{2EA(T)}\right)^{1/n}\left(\frac{a}{c+a}\right)^{1/n} \tag{7}$$

where ρ is density, and g is gravity. We assume the density of pure ice with $\rho = 917$ kg m^{-3} and martian gravity $g = 3.72$ m s^{-2}. The Paterson (1972) model assumes a surface mass-exchange pattern with a zone of uniform accumulation c and a zone of uniform ablation a. Winebrenner et al. (2008) incorporated a variable flowband width into this model, but here we assume that the width is constant. This assumption simplifies our calculations but does not affect the order-of-magnitude estimates presented here.

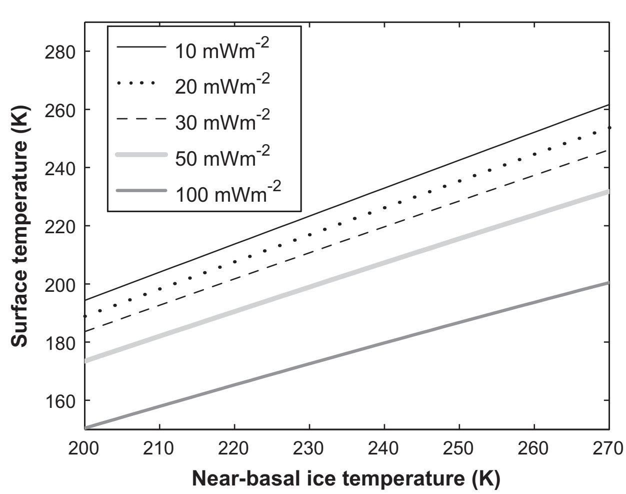

Fig. 3. Surface temperature required to give near-basal ice temperatures from 200 to 270 K for basal heat flux of 10, 20, 30, 50, or 100 mW m^{-2}, calculated using Eq. (4), where thermal conductivity is a function of ice temperature (Eq. (5)).

From Eqs. (6) and (7), the ablation rate a is given by

$$a = \left(\frac{H^2}{L}\right)^{n+1}\frac{(\rho g)^n}{2^n(n+2)}2EA(T)\frac{(1+(c/a))}{(c/a)} \tag{8}$$

Using the ice-flow law exponent n, the accumulation-to-ablation ratio c/a, the maximum ice thickness H, and the flowband length L inferred by Winebrenner et al. (2008) for a characteristic flowband across Gemina Lingula (Table 1), we can calculate the accumulation rate c and the ablation rate a for any combination of ice temperature T and ice-flow enhancement factor E. We note that in these equations the ice thickness is proportional to the 1/8 power (=0.125) of the mass exchange, so the ice thickness is relatively insensitive to the mass exchange. However, the ice-sheet thickness is proportional to the 1/2 power of the length (Eq. (6)). While this is a specific model, it has been chosen because its simplicity can well-describe terrestrial ice sheets (see Winebrenner et al., 2008).

2.4. Response time

The response of ice masses to small perturbations in accumulation or ablation can be estimated using linearized kinematic wave theory (e.g. Nye, 1960; Jóhannesson et al., 1989; Hooke, 2005, Chapter 14; Cuffey and Paterson, 2010, Chapter 11). From this fundamental theory, Jóhannesson et al. (1989) showed that the volume response time for an ice mass to evolve from an initial state to a new steady state after a change in climate could be approximated by

$$\tau_V = \frac{H}{|a(L)|} \tag{9}$$

where H is the maximum ice thickness and $a(L)$ is the ablation rate at the terminus, both in steady state. An ice mass of any ice thickness, with any ice temperature and any ice-flow enhancement, has a corresponding volume response time. The volume response time is the time for volume adjustment of the ice mass after a perturbation in climate or in flow.

Although the entire ice volume is flowing and adjusting to the perturbation, during this process the ice-surface shape approaches a steady-state shape more quickly than the internal-layer shapes do. The characteristic time to establish new steady-state internal stratigraphy is longer than the volume timescale because the ice-sheet must first achieve its new steady-state surface profile and volume (which takes several volume response times), and *then* it has to flush out all of the old layers that were laid down under different climate and strain conditions. There are multiple timescales to characterize ice-sheet behavior, which are fundamental to terrestrial glaciology (e.g. Hooke, 2005, Chapter 14; Cuffey and Paterson, 2010, Chapter 11). The volume response time used here is an order-of-magnitude estimate, for example to discriminate between ice-flow scenarios acting on a 100,000-year timescale compared to a 1 byr timescale.

The difference between the timescale to shape the surface and the timescale to shape the layers (e.g. Hindmarsh, 1996) is important for understanding ice masses on Mars because changes in atmospheric conditions, ice temperature, and/or ice properties are required for a martian ice-surface to approach near-steady flow, yet such changes may not have persisted for long enough to affect internal-layer shapes throughout the ice mass (e.g., Winebrenner et al., 2011, 2012). Our future work will further address how these different response timescales must be considered in any interpretation of martian ice-surface topography and internal-layer shapes.

3. Gemina Lingula, North Polar Layered Deposits (NPLD)

The specific accumulation and ablation (erosion) history across Gemina Lingula is poorly known. While Ivanov and Muhleman (2000) showed that the present-day surface topography across Planum Boreum, NPLD could have been dominantly shaped by ice sublimation, their results were inconclusive across Gemina Lingula. This is consistent with Winebrenner et al. (2008), who showed that Gemina Lingula could have been shaped by a near balance between ice flow and surface mass exchange. Winebrenner et al. (2008) suggested that an era of flow was one of the most recent episodes in Gemina Lingula history, but in order to detect that prior flow the overall surface shape from that era of ice flow must not have been significantly altered. Mass may have been uniformly added or removed across the entire region, or mass may have been locally affected in association with troughs. For example, Milkovich et al. (2008) analyzed NPLD visual stratigraphy and found that the variation across the NPLD in dip and strike of exposed layers at a particular interface could indicate a widespread erosional episode that removed mass so that the remaining surface maintained the same shape. Since we do not know the actual depositional or erosional history of the NPLD, and as discussed by Tanaka et al. (2008) it is likely complicated, it is possible that Planum Boreum and Gemina Lingula experienced similar conditions or it is possible that they experienced different conditions.

Since the accumulation rate, the ablation rate, and the ice temperature during the postulated era of significant ice flow on Mars are all unknown, Winebrenner et al. (2008) used a nondimensionalized model to infer parameter values that would generate ice-surface topography that matched the MOLA data at specific locations along flowbands across Gemina Lingula. The model used by Winebrenner et al. (2008) assumed a simple mass-exchange pattern that consisted of a zone of uniform accumulation c and a zone of uniform ablation a, separated at the equilibrium line R (Paterson, 1972). The parameter values they inferred were the ice-flow law exponent n, the ratio of accumulation rate to ablation rate c/a, the maximum ice thickness H, and the flowband length L. The parameter values from Winebrenner et al. (2008) that we use in this study are given in Table 1.

The primary results of this study are based on inferred parameter values from Winebrenner et al. (2008) that are associated with one characteristic flowband (values in Table 1). We did a sensitivity study of our results to the mass-exchange ratio c/a that is used in this analysis. Winebrenner et al. (2008) inferred $c/a = 0.56$, which is associated with an equilibrium line $R = 0.66$ relative to the flowband length. We compared calculations with $c/a = 0.56$ to calculations with $c/a = 9$ (associated with $R = 0.1$), and with $c/a = 0.1$ (associated with $R = 0.9$); the surface profiles with equilibrium lines at $R = 0.1$, 0.66, and 0.9 are shown in Fig. 2. Using very different mass-exchange patterns, spanning nearly two orders of magnitude, changes our results by less than a factor of 4. Therefore, our results are not very sensitive to the exact value of c/a. In addition, Winebrenner et al. (2008) set up 40 independent problems to infer parameter values for 40 flowbands across Gemina Lingula, and a primary result of their study was that the inferred parameter values were consistent across all flowbands (Fig. 2). Any other candidate processes to explain the large-scale shape of Gemina Lingula must therefore act coherently over a large area in such a way as to mimic the effect of ice flow. In order for an entirely stagnant ice mass to achieve the surface shape of a flowing ice mass, a very specific, and persistent, spatial pattern of mass exchange is required at each point along the entire profile length; this specific mass-exchange pattern must vary with elevation, and an atmospheric mechanism on Mars that would produce this pattern has not yet been identified.

4. Observations

In this section we summarize observations and information that constrain the mass-exchange rate and volume response time for martian ice masses. We discuss how observations from Earth and Mars may determine the role of ice-flow enhancement in the flow of martian ice masses. We also discuss our current understanding of surface-temperature variations and heat flow on Mars, which could warm the near-basal ice compared to the present-day temperature. All of these observations can be used to constrain plausible scenarios where the flow of martian ice masses is more significant. In Section 5 we present the results of our calculations of mass-exchange rate (Eq. (8)) and volume response time (Eq. (9)) that produce the Gemina Lingula surface topography for this plausible range of ice-flow enhancement and ice temperature.

4.1. Constraining the mass-exchange rate

Based on observational estimates of modern accumulation rates (e.g. Laskar et al., 2002; Milkovich and Head, 2005; Fishbaugh and Hvidberg, 2006; Milkovich et al., 2008) and modern ablation rates (e.g. Pathare and Paige, 2005), as well as model-based estimates of past mass-exchange rates (e.g. Levrard et al., 2004), the polar mass-exchange rate on Mars has likely been on the order ~0.1–1 mm/yr over at least the past 10 Myr. Banks et al. (2010) estimate an accumulation rate of 3–4 mm/yr within north polar craters but this is a local accumulation rate relating to the past 10–20 kyr. With an accumulation rate of ~0.1–1 mm/yr and $E = 1$, the near-basal ice temperature must have been ~240–260 K to produce topography similar to that along Gemina Lingula (as shown below in Section 5). Alternatively, with a near-basal ice temperature of ~180 K, the ice-flow enhancement factor must be ~20,000 to equilibrate a mass-exchange rate of 0.1 mm/yr, and ~210,000 to equilibrate a mass-exchange rate of 1 mm/yr. While a near-basal ice temperature of 180 K is plausible, there is no known mechanism to make water ice over ~20,000 times softer. If martian ice flow was ever near steady state, and if ice flow was not substantially enhanced, warmer ice is required to equilibrate a mass-exchange rate ~0.1–1 mm/yr.

4.2. Constraining the volume-response time

In addition to limiting the range of plausible ice temperatures and ice-flow enhancement based on the plausible range of mass-exchange rates, we further constrain pairs of ice temperature and enhancement using the volume response timescale for an ice mass, given by Eq. (9). By putting upper bounds on plausible response times, we put lower bounds on the past mass-exchange rate and the past ice temperature, and/or the enhancement factor. Due to the uncertainty in the age and history of martian ice masses (e.g. Byrne, 2009) we can define only a range of plausible response times that are tied to obliquity variations or to age estimates from crater counts, but large-scale physical processes on Mars could operate on any timescale. Given these uncertainties we think that it is likely that response timescales are less than 100 Myr.

In Section 2.4 we discussed how the volume response time is an upper bound because the ice surface responds faster than the entire volume. As discussed in Section 5, the volume response times associated with near-basal ice temperatures less than ~200 K, without any ice-flow enhancement, are physically implausible; these temperatures imply response times that are older than the age of the planet. We expect that for flow to shape martian ice masses on plausible timescales that flow was enhanced and ice temperature was warmer.

4.3. The role of ice-flow enhancement

The ice-flow enhancement scaling factor in the ice-flow law that we use here can account for variations in the physical properties of ice, such as grain size, crystal orientation, and impurity content that can enhance or retard the strain rate compared to the value calculated by the isotropic creep relation (e.g. Cuffey and Paterson, 2010, p. 71). When these variations are concentrated in the basal layer of a glacier or ice sheet, their effect on ice-flow rate can be especially significant (e.g. Knight, 1997). In our calculations, we assumed that deformation occurred entirely by creep, and that there was no sliding at the base. However, a liquid brine-, water- or till-lubricated base could cause sliding that would significantly quicken the rate of ice flow. Fisher et al. (2010) proposed that the NPLD could experience enhanced flow by sliding over perchlorate sludge. While this may be a viable hypothesis, we focus our discussion on mechanisms that enhance the rate of internal deformation. We briefly review how anisotropy and impurity content affect the rate of ice deformation on Earth, and we consider how these mechanisms may be relevant to ice deformation on Mars.

On Earth the enhancement factor typically accounts for changes in the creep rate for anisotropic ice compared to isotropic ice at the same stress and temperature. Most terrestrial ice masses are anisotropic to some degree at some depths, but ice sheets are often considered to be isotropic to simplify theoretical studies of their behavior. While sophisticated flow laws that incorporate enhancement from anisotropy have been developed (e.g. Azuma, 1994), an enhancement factor is a simple way to account for any mechanism, including anisotropy, that changes the flow rate. The enhancement factor represents enhancement in the dominant strain-rate component and also depends on the mechanism of deformation, varying for different values of the flow-law exponent n. Here we focus on scaling the flow law for ice with $n = 3$.

Analysis of ice cores has shown that crystal anisotropy can change the rates of shear parallel to the basal plane by a factor of 10 (e.g. Cuffey and Paterson, 2010, p. 87), and therefore it is important to account for this effect. While crystal fabric plays a role in either enhancing or retarding ice deformation, the impurity content of the ice is also important. In addition, for terrestrial ice sheets the overall dust content is still low, and while dust has a relatively minor influence on ice rheology, the presence of fine particles may soften the ice. Although Durham et al. (2009) showed that the relative viscosity of icy sand packs with an ice fraction less than 50% is much greater than that of pure ice, the strength of nearly-pure ice containing smaller amounts of sand can be less than the strength of pure ice, increasing the creep rate (e.g. Cuffey, 2000; Fitzsimons et al., 2001). This agrees with tunnel-closure observations, which detected localized enhanced deformation of the debris-rich basal layers of Taylor Glacier, Antarctica (e.g. Fitzsimons et al., 1999; Samyn et al., 2005). It also agrees with modeling of the observed strain rates at Taylor Glacier (E. Whorton, personal communication inferred enhancement factors >40), with measurements from a glacier in China (Echelmeyer and Zhongxiang, 1987; measured enhancement factors ∼100), with basal ice from the Byrd, Antarctica ice core (e.g. Gow et al., 1968), and with studies of the basal ice at Meserve Glacier, Antarctica (e.g. Cuffey, 2000). We use observations of terrestrial ice-flow enhancement due primarily to anisotropy or basal debris as a guide to choose a range of ice-flow enhancement factors for our martian calculations. While some terrestrial enhancement mechanisms may act on Mars, in this study we can determine only a range of plausible enhancement factors that will inform separate studies of martian enhancement mechanisms.

For example, ice-flow enhancement on Mars may be primarily due to impurities rather than to anisotropy or debris content. The Phoenix lander found perchlorate in the surface soil at ∼68°N (e.g. Hecht et al., 2009), and even though the distribution and mode of formation of the perchlorate remains unknown, Catling et al. (2010) proposed an origin similar to arid environments on Earth. There may be a higher concentration of perchlorate in polar soil (Massé et al., 2010), which could become further concentrated by thin films of liquid water (Cull et al., 2010). Given that the PLD are probably partially derived from this polar soil, perchlorate is likely to be a PLD constituent. Perchlorate is highly water soluble, and could depress the freezing point as much as 70 °C for a brine mixture (Hecht et al., 2009; Fisher et al., 2010). Lenferink et al. (2012) conducted lab experiments of perchlorate-laden ice and observed flow enhancement even at 2% perchlorate concentration, and they suggested that such enhancement might also occur at lower concentrations.

In contrast to basal entrainment of perchlorate, carbon dioxide (CO_2) ice precipitates out of the martian atmosphere. While it is likely that it is only a relatively minor constituent of the PLD (e.g. Nye et al., 2000), CO_2 ice or clathrate hydrate, if present, could influence the rate of ice flow. Phillips et al. (2011) identified a shallow subsurface CO_2 deposit in the SPLD, and we cannot rule out the possibility that the NPLD had a buried CO_2 deposit in the past or has a present layer that has not yet been identified. Durham et al. (2000) demonstrated that CO_2 ice is weaker than water ice, but that clathrate hydrate is stronger, and also has a lower conductivity. While we have no direct evidence from the PLD, Delory et al. (2006) reported that martian dust storms may generate strong enough electrostatic fields to dissociate CO_2 and H_2O, to eventually form hydrogen peroxide (H_2O_2) that subsequently falls out of the martian atmosphere. Dust storms of all scales are omnipresent on Mars, and the largest dust storms typically occur during perihelion, when Southern hemisphere summer temperatures are relatively high (e.g. Martin and Zurek, 1993). If hydrogen peroxide snow, or any other chemical constituent, is entrained in Northern hemisphere winter precipitation, this could change the hardness, and therefore the deformation rate of the PLD ice relative to pure H_2O ice. Li et al. (2009) showed that sulfuric acid (H_2SO_4) reduces the strength of ice proportional to the square root of the sulfuric acid concentration; they showed that sulfuric acid was more effective at softening the ice at lower temperature.

In summary, terrestrial observations show that ice-flow enhancement ranges from $E \sim 0.9$ to 50+ (e.g. Cuffey and Paterson, 2010, p. 77), with maximum observed values over 100 (e.g. Echelmeyer and Zhongxiang, 1987; Cuffey and Paterson, 2010, p. 315). On Earth the highest enhancement is exhibited in the basal layers and is usually related to debris content or crystal anistropy. While it is unlikely that large martian ice masses with nearly pure water ice have been temperate, impurities such as perchlorate in the ice would facilitate flow at lower temperatures (e.g. Hecht et al., 2009; Fisher et al., 2010; Lenferink et al., 2012).

4.4. Variations in basal-ice temperature

Terrestrial heat-flux variations can be surprisingly large. For example, although typical terrestrial heat flow on the continents is around 50 mW m^{-2}, basal melting at the base of the North Greenland Ice-Core Project (NGRIP) site required a heat flux of ∼130 mW m^{-2} (e.g. Fahnestock et al., 2001; NGRIP members, 2004; Buchardt and Dahl-Jensen, 2007). On Mars, the present-day planetary heat flux was been estimated at 20–30 mW m^{-2} (e.g. Clifford, 1993; Grott et al., 2007), but the actual value and its spatial variation (e.g. Zuber et al., 2000) are poorly known especially in the past.

What heat flux is required to warm the basal ice to 230 K? For a specified surface temperature, and using Eq. (4), we can calculate the heat flux that gives an ice temperature of 230 K at 1800 m depth (near the base of a 1900 m-thick ice mass). For a surface temperature of 170 K, a heat flux of 95 mW m^{-2} is required to reach 230 K at 1800 m depth, and for a surface temperature of 200 K, a heat flux 45 mW m^{-2} is required. Combinations of surface temperature, near-basal temperature, and heat flux are shown in Fig. 3. If there was a region of higher heat flux in the geologically recent martian past, it is presumed to be due to a transient tecton-o-thermal or volcanic event (e.g. Clifford, 1987; Benito et al., 1997; Anguita et al., 2000; Fishbaugh and Head, 2002; Hovius et al., 2008). We do not address the plausibility or timing of such a thermal event here, but achieving a heat flux of approximately 50–100 mW m^{-2} may be reasonable.

Albedo is important because surface temperature depends on the fraction of incoming shortwave radiation from the Sun that is absorbed by the surface. Mischna and Richardson (2005) showed that the polar ice caps must be insulated at high obliquity in order to avoid completely subliming away, and that the polar contribution to the global water budget is limited at high obliquity. Levrard et al. (2007) also found that NPLD ice was unstable at high obliquity ($\sim$30–35°), whenever the absorbed insolation was greater than 300 W m^{-2}. Unless an efficient dust-lag deposit formed to protect the NPLD, the north-polar ice would quickly sublimate and redeposit in the mid-latitudes during the high-obliquity conditions from 10 to 4 Myr ago because the seasonal sublimation rates during high obliquity are an order of magnitude greater than the seasonal accumulation rates. Unless the entire NPLD are less than $\sim$4 Myr old, protection of at least some portion of the NPLD from higher insolation 10 to 4 Myr ago, and possibly for many millions or billions of years, must have occurred. We know that a dust-lag deposit has effectively protected the SPLD from complete sublimation during high obliquity because the surface exposure age of the SPLD is 100 to 30 Myr (e.g. Plaut et al., 1988; Herkenhoff and Plaut, 2000; Koutnik et al., 2002), and the present-day South PLD surface has a very low thermal inertia that indicates dust cover (e.g. Paige and Keegan, 1994; Vasavada et al., 2000). The South PLD has also received $\sim$4–11% more insolation on an annual average over the past 20 Myr because of the eccentricity of Mars' orbit (from calculations by Laskar et al. (2004)). However, the nature of the preserved cratering record, where the floors of craters greater than $\sim$800 m in diameter have viscously relaxed (e.g. Pathare et al., 2005), but the crater rims have been maintained (e.g. Koutnik et al., 2002; Pathare et al., 2005), attests to the efficiency of the lag deposit in preserving the underlying ice. If the sublimation rate at the South Pole was $\sim$0.2 mm/yr, a rim height of $\sim$10 m would be removed in less than 50,000 years, which has not been the case. The thickness of the lag deposit is minimally $\sim$5 mm (e.g. Skorov et al., 2001), could be $\sim$50 cm (e.g. Paige and Keegan, 1994; Ellehøj et al., 2007), but the actual thickness is unknown and the lag deposit could be thicker. The present-day state of the SPLD is an indication that the dust-lag deposit has protected the underlying ice for many millions of years. Mid-latitude observations of near-surface exposed ice in recent craters (e.g. Byrne et al., 2009), as well at the Phoenix landing site (e.g. Smith et al., 2009), indicate that ice can be stable buried only a few centimeters below the surface.

Surface temperatures at the North Pole, subject to orbital-parameter variations over the past 10 Myr, have been calculated (e.g. Pathare and Paige, 2005; Levrard et al., 2007; Schorghofer, 2008), and the annual-average surface temperature at 80–90°N was always below $\sim$180 K. Pathare and Paige (2005) showed that the summertime maximum temperature at the North Pole was $\sim$220 K, and could even reach $\sim$270 K depending on the perihelion configuration, obliquity, and eccentricity. Despite these relatively warm summertime temperatures, the annual-average temperature is very low because cold wintertime temperatures lead to CO_2 frost precipitating out of the atmosphere with a 7 mbar frost-point temperature of 148 K (Kieffer et al., 1976). Annual-average surface temperatures would be higher if there was a reduction in the extent or duration of seasonal CO_2 deposition across the North PLD. There would be further warming of the surface if there was a decrease in surface albedo from a dust-lag deposit, which must have been present if the North PLD survived the last period of high obliquity from 10 to 4 Ma (e.g. Mischna and Richardson, 2005; Levrard et al., 2007). However, to affect the rate of ice flow, changes in surface temperature must propagate to the near-basal ice, and this deep ice warms by diffusion (e.g. Larsen and Dahl-Jensen, 2000). Fig. 4b shows how the diffusion time for a 1900 m thick ice mass can range from $\sim$115 to 25 ka depending on the thermal parameters. The diffusion timescale is defined by the depth z of the propagation of the thermal wave and by the thermal diffusivity κ

$$\tau_d = \frac{z^2}{\kappa} \tag{10}$$

where $\kappa = k/\rho c$ is a function of temperature with thermal conductivity k given by Eq. (5), density ρ, and specific heat capacity c as a function of temperature T given by (e.g. Cuffey and Paterson, 2010, p. 400; illustrated in Fig. 4a):

$$c(T) = 152.5 + 7.122T \tag{11}$$

Therefore, a change in surface temperature must be sustained on a timescale similar to the diffusion time to give a change in near-basal temperature.

5. Results

5.1. Present-day rates of ice flow on Gemina Lingula, NPLD

The present-day mean annual surface temperature of the North PLD is $\sim$162 K (e.g. Pathare and Paige, 2005; Levrard et al., 2007; Schorghofer, 2008), the present-day average ablation rate is estimated to be $\sim$0.2 mm/yr (e.g. Pathare and Paige, 2005), and the present-day average accumulation rate is estimated to be $\sim$0.5–0.6 mm/yr (e.g. Laskar et al., 2002; Milkovich and Head, 2005). For surface temperature of 162 K, and assuming a heat flux of 30 mW m^{-2} (e.g. Clifford, 1993) the ice temperature at a depth of 1900 m is $\sim$177 K. Using these values, Fig. 5 shows the surface shape of a steady-state flowing ice mass calculated using Eqs. (6) and (7) with a maximum ice thickness of 1900 m, a surface

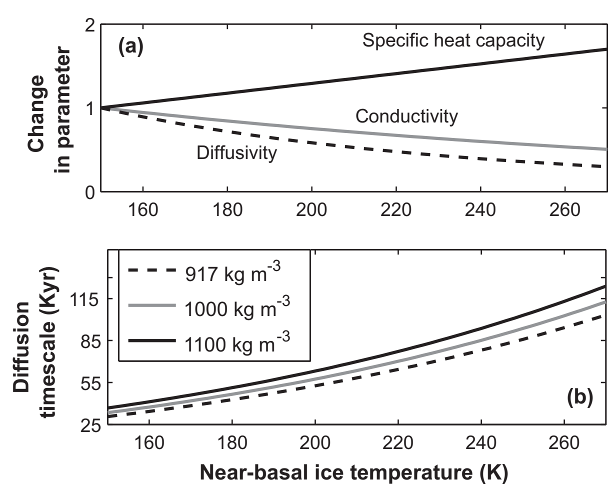

Fig. 4. (a) Specific heat capacity c (Eq. (11)), thermal conductivity k (Eq. (5)), and thermal diffusivity $\kappa = k/\rho c$ as a function of ice temperature, all normalized by their values at 150 K. (b) Characteristic timescale for diffusion (Eq. (10)) as a function of near-basal ice temperature for ice density ρ = 917 kg m^{-3}, 1000 kg m^{-3}, and 1100 kg m^{-3}.

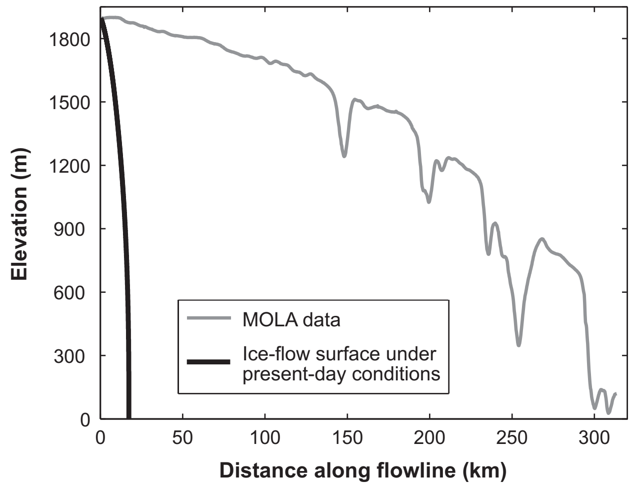

Fig. 5. Thick black line shows the steady-state ice surface calculated with a surface temperature $T = 170$ K, an accumulation rate $c = 0.5$ mm/yr, and an ablation rate $a = 0.2$ mm/yr. Gray line shows the present-day MOLA topography along the study flowband on Gemina Lingula, NPLD. Compared to the fits by Winebrenner et al. (2008) to this MOLA topography, the model surface slopes must be very high for ice flow to balance the relatively high modern mass flux and cold ice.

temperature of 162 K, an accumulation rate of 0.5 mm/yr, and with a mass-exchange ratio $c/a = 0.56$. This surface shape is compared to the MOLA topography along a profile across Gemina Lingula and unlike the results from Winebrenner et al. (2008) these surfaces are very different. Present-day martian surface temperature is too cold, and the mass-exchange rates are too high (even though the actual values are physically very low) to develop the present-day topography across Gemina Lingula. In order for ice flow to be significant at very cold temperature, and to equilibrate this rate of accumulation, the surface slopes have to be very high. It has already been shown that present-day ice flow has an insignificant affect on the surface topography, and except near steep trough faces (e.g. Hvidberg, 2003) martian ice must have been warmer to flow at a significant rate (e.g. Greve et al., 2004); Fig. 5 emphasizes this result.

5.2. Mass-exchange rate and volume response time for Gemina Lingula, NPLD

To constrain the conditions necessary to facilitate ice flow, we constrain the plausible range of mass-exchange rates and the plausible range of volume response timescales associated with pairs of ice temperature and ice-flow enhancement. The ice temperature that we prescribe is the near-basal ice temperature, because this is the value that is important for ice deformation. We consider near-basal ice temperatures from 180 to 260 K, and we consider ice-flow enhancement factors from $E = 1$ to 100; the range of E is chosen based on terrestrial experience (e.g. Echelmeyer and Zhongxiang, 1987; Cuffey, 2000; E. Whorton, personal communication; Cuffey and Paterson, 2010, p. 77) and the physical significance of E is discussed in Section 4.3. All rates are given in Earth years.

To calculate the mass-exchange rate and the volume response time, we use the mass-exchange ratio of accumulation rate over ablation rate $c/a = 0.56$, ice thickness $H = 1900$ m, length $L \sim 317$ km, and the ice-flow law exponent $n = 3$ inferred by Winebrenner et al. (2008) from a characteristic flowband along Gemina Lingula (Table 1). We calculate the ablation rate using Eq. (8), and we calculate the volume response time using Eq. (9). The ablation rate required for steady state scales linearly with the ice-flow enhancement factor E, and the ice-softness parameter $A(T)$ follows an Arrhenius relation (Eq. (3)). Fig. 6 shows the ablation rate a required for steady state (where the accumulation rate $c = 0.56a$) and the volume response time τ for all pairs of ice temperature $T = 180$–260 K and enhancement factor $E = 1$–100 for an ice mass with maximum thickness $H = 1900$ m. The boxed region in Fig. 6 indicates the range of enhancement and ice temperature associated with response timescales from ~1 to 100 Myr. Table 2 gives the exact values for select pairs from Fig. 6.

Scenario 1 in Table 2 shows that the present-day ice temperature is too cold to produce surface topography similar to Gemina Lingula because it requires a mass-exchange rate that is too low and a volume response time that is too high. Scenarios 2 and 3 in Table 2 show that moderate increases in ice temperature and in ice-flow enhancement give plausible mass-exchange rates and volume response times. Response times less than 5 Myr require ice temperatures at least 220–230 K in addition to enhancement of

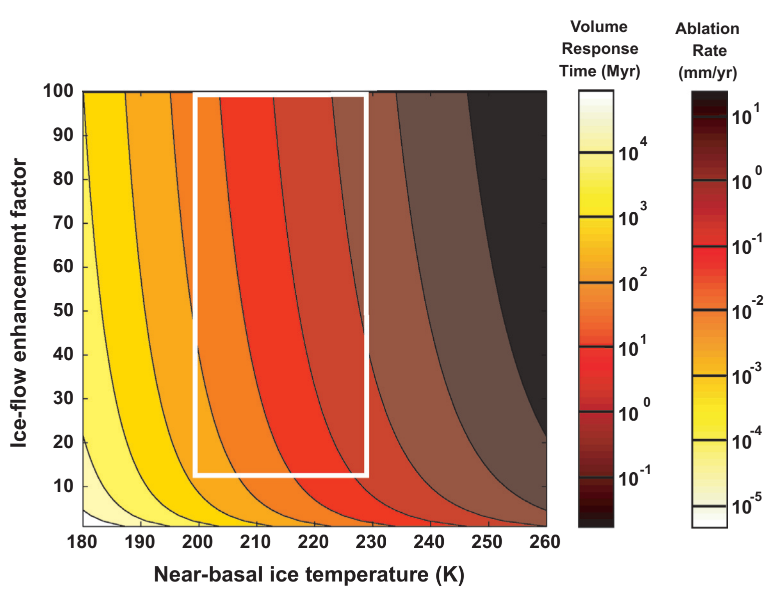

Fig. 6. Contours of volume response time (from Eq. (9)) and ablation rate (from Eq. (8)) for all pairs of near-basal ice temperature $T = 180$–260 K, and ice-flow enhancement factor $E = 1$–100 for an ice mass with maximum thickness $H = 1900$ m and all other parameters given in Table 1. We consider that scenarios with near-basal temperature from ~200 to 230 K with ice-flow enhancement greater than 10 give plausible volume response times ~1–100 Myr (this range is roughly highlighted with the white box).

Table 2
Ice flow and climate scenarios.

Scenario	Near-basal ice temperature (K)	Ice-flow enhancement factor	Ablation rate (mm/yr)	Volume response time
1	180	1	4.7×10^{-6}	403 Byr
2	215	10	0.032	59 Myr
3	230	50	1.4	1.3 Myr

Calculated values for three example scenarios from Fig. 6 that have different near-basal ice temperatures and different ice-flow enhancement factors. Ablation rate is calculated using Eq. (8) and volume response time is calculated using Eq. (9). All three scenarios use parameter values from Winebrenner et al. (2008) given in Table 1. Warmer ice with higher ice-flow enhancement will respond faster, and is balanced by a higher mass-exchange rate.

10–50, and greater ice-flow enhancement can facilitate colder ice to flow on the same timescale.

There is general agreement that at least some ice masses on Mars have been shaped by ice flow. For example, Lobate Debris Aprons (e.g. Colaprete and Jakosky, 1998; Mangold and Allemand, 2001; Holt et al., 2008; Plaut et al., 2009) and smaller-scale viscous flow features (e.g. Milliken et al., 2003) are found predominantly in the mid-latitudes. Most of these features are much smaller than Gemina Lingula and, more importantly, they are found in different physical environments. The bedrock beneath Gemina Lingula is relatively flat, especially relative to the ice thickness, but other ice masses may not have flat beds. So, scaling this analysis from Gemina Lingula to other smaller martian ice masses may not always be appropriate. However, this analysis can be redone to address specific questions about climate and ice-flow conditions for other ice masses. If all of the parameters required for this analysis (Table 1) have not been inferred directly on other ice masses (e.g. following Winebrenner et al., 2008), we suggest that the thickness and length of another ice mass be used together with the mass-exchange pattern c/a and flow-law exponent n inferred for Gemina Lingula. Sensitivity analysis of the mass-exchange pattern could be done by using $c/a = 0.1$–9, associated with equilibrium line positions $R = 0.1$–0.9 along the profile length (Fig. 2), which we did for Gemina Lingula and found that our response timescale results changed by less than a factor of 4. This way the volume response as a function of ice temperature and ice-flow enhancement may be estimated directly for other ice masses from their ice thickness and length.

6. Conclusions

Warmer near-basal ice temperatures, most likely in combination with enhanced ice flow, are required for near-steady flow to generate topography with the shape characteristic of topography across Gemina Lingula, NPLD in a reasonable amount of time (e.g. less than 100 Myr), and with a plausible rate of mass exchange. We do not propose a specific mechanism, or combination of mechanisms, that could warm the ice or enhance the flow, but we present a range of combinations of ice temperature and ice-flow enhancement that can inform future analyses of PLD geometry, internal structure, and ice rheology. The volume response time is a way to assess the feasibility of any mechanism that may promote ice to flow faster. In summary:

(1) While interpreting ice-surface topography is also dependent on model assumptions about ice flow, the surface shape is not dependent on details of the mass-exchange pattern. There are many histories that can create equivalent surface shapes; if ice flowed it has a predictable shape.
(2) Our analysis is an important extension of Winebrenner et al. (2008) because the radar-based arguments against ice flow and specific tests of flow hypotheses are by their nature inconclusive, and any episode of ice flow required conditions different than present-day Mars.
(3) For Gemina Lingula to be shaped by ice flow in a plausible amount of time, our calculations indicate that near-basal ice must have been moderately warmer (200–230 K), and that ice flow was likely significantly enhanced (by at least a factor of 10). We present combinations of ice temperature and flow enhancement that can be compared to other investigations of specific mechanisms to warm the ice and/or enhance the flow.
(4) There is general agreement that the shape of other features on Mars indicates that they flowed in the past, for example Lobate Debris Aprons (e.g. Colaprete and Jakosky, 1998; Mangold and Allemand, 2001; Holt et al., 2008; Plaut et al., 2009). Our analysis of volume response as a function of ice temperature and ice-flow enhancement can be extended to other ice masses.

Acknowledgments

This work was supported by NASA Grant NNX09AI48G and by an NSF International Research Fellowship Program award 0853407 to M.R.K. We thank Thomas Neumann for input during the initial stages of this work. We thank Stephen Clifford and Jeffrey Moersch for editing this manuscript, and we acknowledge two anonymous reviewers for their constructive comments to improve the manuscript.

References

Anguita, F., Babin, R., Benito, G., Gomez, D., Collado, A., Rice, J.W., 2000. Chasma Australe, Mars: Structural framework for a catastrophic outflow origin. Icarus 144, 302–312.
Armstrong, J.C., Titus, T.N., Kieffer, H.H., 2005. Evidence for subsurface water ice in Korolev crater, Mars. Icarus 175, 360–372.
Azuma, N., 1994. A flow law for anisotropic ice and its applications to ice sheets. Earth Planet. Sci. Lett. 128, 601–614.
Banks, M.E., Pelletier, J.D., 2008. Forward modeling of ice topography on Mars to infer basal shear stress conditions. J. Geophys. Res. 113. http://dx.doi.org/10.1029/2007JE002895.
Banks, M.E. et al., 2010. Crater population and resurfacing of the martian North Polar Layered Deposits. J. Geophys. Res. 115. http://dx.doi.org/10.1029/2009JE003523.
Benito, G., Mediavilla, F., Fernandez, M., Marquez, A., Martinez, J., Anguita, F., 1997. Chasma Boreale, Mars: A sapping and outflow channel with a tectono-thermal origin. Icarus 129, 528–538.
Bourke, M.C., Balme, M., Beyer, M., Williams, K.K., Zimbelman, J., 2006. A comparison of methods used to estimate the height of sand dunes on Mars. Geomorphology 81, 440–452.
Buchardt, S.L., Dahl-Jensen, D., 2007. Estimating the basal melt rate at NorthGRIP using a Monte Carlo technique. Ann. Glaciol. 45, 137–142.
Byrne, S., 2009. The polar deposits of Mars. Annu. Rev. Earth Planet. Sci. 37, 535–560.
Byrne, S. et al., 2009. Distribution of mid-latitude ground-ice on Mars from new impact craters. Science 325, 1674.
Catling, D.C. et al., 2010. Atmospheric origins of perchlorate on Mars and in the Atacama. J. Geophys. Res. 115. http://dx.doi.org/10.1029/2009JE003425.
Clifford, S.M., 1987. Polar basal melting on Mars. J. Geophys. Res. – Solid Earth Planets 92, 9135–9152.
Clifford, S.M., 1993. A model for the hydrologic and climatic behavior of water on Mars. J. Geophys. Res. 98, 10973–11016.
Colaprete, A., Jakosky, B.M., 1998. Ice flow and rock glaciers on Mars. J. Geophys. Res. 103, 5897–5909.

Cuffey, K.M., 2000. Methodology for use of isotopic climate forcings in ice sheet models. Geophys. Res. Lett. 27 (19), 3065–3068.

Cuffey, K., Paterson, W.S.B., 2010. The Physics of Glaciers, fourth ed. Elsevier, Burlington, MA.

Cull, S.C. et al., 2010. Concentrated perchlorate at the Mars Phoenix landing site: Evidence for thin film liquid water on Mars. Geophys. Res. Lett. 37. http://dx.doi.org/10.1029/2010GL045269.

Delory, G.T. et al., 2006. Oxidant enhancement in martian dust devils and storms: Storm electric fields and electron dissociative attachment. Astrobiology 6 (3), 451–462.

Dickson, J.L., Head, J.W., Fassett, C.I., 2012. Patterns of accumulation and flow of ice in the mid-latitudes of Mars during the Amazonian. Icarus 219, 723–732.

Durham, W.B., Kirby, S.H., Stern, L.A., 2000. Comparative rheologies of solid H_2O, CO_2, and CO_2 clathrate hydrate. In: Second International Conference on Mars Polar Science and Exploration, Rekjavik, Iceland (abstract).

Durham, W.B., Pathare, A.V., Stern, L.A., Lenferink, H.J., 2009. Mobility of icy sand packs, with application to martian permafrost. Geophys. Res. Lett. 36, http://dx.doi.org/1029/2009GL040392.

Echelmeyer, K., Zhongxiang, Wang., 1987. Direct observation of basal sliding and deformation of basal drift at sub-freezing temperatures. J. Glaciol. 33 (113), 83–98.

Ellehøj, M.D., 2007. Subsurface Ice on Mars: A Study on Ground Ice Stability and Applications. Master Thesis, University of Copenhagen. 158pp.

Fahnestock, M., Abdalati, W., Joughin, I., Brozena, J., Gogineni, P., 2001. High geothermal heat flow, basal melt, and the origin of rapid ice flow in central Greenland. Science 294, 2338–2342.

Fastook, J.L., Head, J.W., Marchant, D.R., Forget, F., Madeleine, Jean-Baptiste, 2012. Early Mars climate near the Noachian-Hesperian boundary: Independent evidence for cold conditions from basal melting of the south polar ice sheet (Dorsa Argentea Formation) and implications for valley network formation. Icarus 219, 25–40.

Fishbaugh, K.E., Head, J.W., 2002. Chasma Boreale, Mars: Topographic characterization from Mars Orbiter Laser Altimeter data and implications for mechanisms of formation. J. Geophys. Res. – Planets 107. http://dx.doi.org/10.1029/2000JE001351.

Fishbaugh, K.E., Hvidberg, C.S., 2006. Martian North Polar Layered Deposits stratigraphy: Implications for accumulation rates and flow. J. Geophys. Res. – Planets 111. http://dx.doi.org/10.1029/2005JE002571.

Fisher, D.A., Hecht, M.H., Kounaves, S.P., Catling, D.C., 2010. J. Geophys. Res., 115. http://dx.doi.org/10.1029/2009JE003405.

Fitzsimons, S.J., Mcmanus, K.J., Lorrain, R.D., 1999. Structure and strength of basal ice and substrate of a dry-based glacier: Evidence for substrate deformation at sub-freezing temperatures. Ann. Glaciol. 28, 236–240.

Fitzsimons, S.J., Mcmanus, K.J., Sirota, P., Lorrain, R.D., 2001. Direct shear tests of materials from a cold glacier: Implications for landform development. Quatern. Int. 86, 129–137.

Glen, J.W., 1955. The creep of polycrystalline ice. Proc. R. Soc. Lond. Ser. A – Math. Phys. Sci. 228 (1175), 519–538.

Gow, A.J., Ueda, H.T., Garfield, D.E., 1968. Antarctic ice sheet – Preliminary results of first core hole to bedrock. Science 161 (3845), 1011–1013.

Greve, R., Mahajan, R.A., Segschneider, J., Grieger, B., 2004. Evolution of the north-polar cap of Mars: A modelling study. Planet. Space Sci. 52 (9), 775–787.

Grott, M., Helbert, J., Nadalini, R., 2007. Thermal structure of martian soil and the measurability of the planetary heat flow. J. Geophys. Res. – Planets 112. http://dx.doi.org/10.1029/2007JE002905.

Head, J.W. et al., 2005. Tropical to mid-latitude snow and ice accumulation, flow and glaciation on Mars. Nature 434, 346–351.

Hecht, M.H. et al., 2009. Detection of perchlorate and the soluble chemistry of martian soil at the Phoenix lander site. Science 325, 64–67.

Herkenhoff, K.E., Plaut, J.J., 2000. Surface ages and resurfacing rates of the polar layered deposits on Mars. Icarus 144, 243–253.

Hindmarsh, R.C.A., 1996. Stochastic perturbation of divide position. Ann. Glaciol. 23, 94–104.

Hindmarsh, R.C.A., Leysinger Vieli, G.J.-M.C., Raymond, M.J., Gudmundsson, G.H., 2006. Draping or overriding: The effect of horizontal stress gradients on internal layer architecture in ice sheets. J. Geophys. Res. 111. http://dx.doi.org/10.1029/2005JF000309.

Holt, J.W. et al., 2008. Radar sounding evidence for buried glaciers in the southern mid-latitudes of Mars. Science 322, 1235–1238.

Holt, J.W., Smith, I.B., Christian, S., Brothers, T.C., Phillips, R.J., 2011. Radar stratigraphy of Planum Boreum, Mars: A rich history of accumulation and erosion preserved by a lack of flow. Lunar Planet. Sci. XLII, 2664 (abstract).

Hooke, R.L., 2005. Principles of Glacier Mechanics, second ed. Cambridge University Press.

Hovius, N., Lea-Cox, A., Turowski, J.M., 2008. Recent volcano-ice interaction and outburst flooding in a Mars polar cap re-entrant. Icarus 197 (1), 24–38.

Hvidberg, C.S., 2003. Relationship between topography and flow in the north polar cap on Mars. Ann. Glaciol. 37, 363–369.

Ivanov, A.B., Muhleman, D.O., 2000. The role of sublimation for the formation of the northern ice cap: Results from the Mars Orbiter Laser Altimeter. Icarus 144, 436–448.

Jóhannesson, T., Raymond, C., Waddington, E., 1989. Time-scale for adjustment of glaciers to changes in mass balance. J. Glaciol. 35 (121), 355–369.

Karlsson, N.B., Holt, J.W., Hindmarsh, R.C.A., 2011. Testing for flow in the North Polar Layered Deposits of Mars using radar stratigraphy and a simple 3D ice-flow model. Geophys. Res. Lett. 38. http://dx.doi.org/10.1029/2011GL049630.

Kieffer, H.H., Chase, S.C., Martin, T.Z., Miner, E.D., Palluconi, F.D., 1976. Martian North Pole summer temperatures – Dirty water ice. Science 194 (4271), 1341–1344.

Knight, P.G., 1997. The basal ice layer of glaciers and ice sheets. Quatern. Sci. Rev. 16 (9), 975–993.

Koutnik, M., Byrne, S., Murray, B., 2002. South Polar Layered Deposits of Mars: The cratering record. J. Geophys. Res. – Planets 107 (E11). http://dx.doi.org/10.1029/2001JE001805.

Koutnik, M., Waddington, E., Winebrenner, D.P., 2009. A method to infer past surface mass balance and topography from internal layers in martian polar layered deposits. Icarus 204, 458–470.

Lancaster, N., 1995. Geomorphology of Desert Dunes. Routeledge, London.

Larsen, J., Dahl-Jensen, D., 2000. Interior temperatures of the northern polar cap on Mars. Icarus 144, 456–462.

Laskar, J., Levrard, B., Mustard, J.F., 2002. Orbital forcing of the martian polar layered deposits. Nature 419 (6905), 375–377.

Laskar, J., Correia, A.C.M., Gastineau, M., Joutel, F., Levrard, B., Robutel, P., 2004. Long term evolution and chaotic diffusion of the insolation quantities of Mars. Icarus 170 (2), 343–364.

Lenferink, H.J., Durham, W.B., Stern, L.A., Pathare, A.V., 2012. Weakening of ice by magnesium perchlorate hydrate. Icarus.

Levrard, B., Forget, F., Montmessin, F., Laskar, J., 2004. Recent ice-rich deposits formed at high latitudes on Mars by sublimation of unstable equatorial ice during low obliquity. Nature 431 (7012), 1072–1075.

Levrard, B., Forget, F., Montmessin, F., Laskar, J., 2007. Recent formation and evolution of northern martian polar layered deposits as inferred from a Global Climate Model. J. Geophys. Res. – Planets 112 (E6). http://dx.doi.org/10.1029/2006JE002772.

Leysinger Vieli, G.J.-M.C., Hindmarsh, R.C.A., Siegert, M.J., Bo, S., 2011. Time-dependence of the spatial pattern of accumulation rate in East Antarctica deduced from isochronic radar layers using a 3-D numerical ice flow model. J. Geophys. Res. 116. http://dx.doi.org/10.1029/2010JF001785.

Li, X., Iliescu, D., Baker, I., 2009. On the effects of temperature on the strength of H_2SO_4-doped ice single crystals. J. Glaciol. 55 (191), 481–484.

Mangold, N., Allemand, P., 2001. Topographic analysis of features related to ice on Mars. Geophys. Res. Lett. 28, 407–410.

Martin, L.J., Zurek, R.W., 1993. An analysis of the history of dust activity on Mars. J. Geophys. Res. 98, 3221–3246.

Massé, M., Bourgeois, O., Le Mouélic, S., Verpoorter, C., Le Deit, L., Bibring, J.P., 2010. Martian polar and circum-polar sulfate-bearing deposits: Sublimation tills derived from the north polar cap. Icarus 209, 434–451.

Milkovich, S.M., Head, J.W., 2005. North polar cap of Mars: Polar layered deposit characterization and identification of a fundamental climate signal. J. Geophys. Res. – Planets 110 (E1). http://dx.doi.org/10.1029/2004JE002349.

Milkovich, S.M., Head, J.W., Neukum, G., HRSC Co-Investigator Team, 2008. Stratigraphic analysis of the northern polar layered deposits of Mars: Implications for recent climate history. Planet. Space Sci. 56, 266–288.

Milliken, R.E., Mustard, J.F., Goldsby, D.L., 2003. Viscous flow features on the surface of Mars: Observations from high-resolution Mars Orbiter Camera (MOC) images. J. Geophys. Res. 108. http://dx.doi.org/10.1029/2002JE002005.

Mischna, M.A., Richardson, M.I., 2005. A reanalysis of water abundances in the martian atmosphere at high obliquity. Geophys. Res. Lett. 32 (3). http://dx.doi.org/10.1029/2004GL02.

Ng, F.S.L., Barr, I.D., Clark, C.D., 2010. Using the surface profiles of modern ice masses to inform palaeo-glacier reconstructions. Quatern. Sci. Rev. 29, 3240–3255.

NGRIP members, 2004. High-resolution record of Northern Hemisphere climate extending into the last interglacial period. Nature 431 (7005), 147–151.

Nye, J.F., 1957. The distribution of stress and velocity in glaciers and ice sheets. Proc. R. Soc. Lond. Ser. A 239, 113–133.

Nye, J.F., 1960. The response of glaciers and ice-sheets to seasonal and climatic changes. Proc. R. Soc. Lond. Ser. A 256 (1287), 559–584.

Nye, J.F., Durham, W.B., Schenk, P.M., Moore, J.M., 2000. The instability of a south polar cap on Mars composed of carbon dioxide. Icarus 144, 449–455.

Paige, D.A., Keegan, K.D., 1994. Thermal and albedo mapping of the polar-regions of Mars using Viking Thermal Mapper observations 2. South polar-region. J. Geophys. Res. – Planets 99 (E12), 25993–26013.

Parsons, R.A., Nimmo, F., Miyamoto, H., 2011. Constraints on martian lobate debris apron evolution and rheology from numerical modeling of ice flow. Icarus 214, 246–257.

Paterson, W.S.B., 1969. The Meighen Ice Cap, Arctic Canada: Accumulation, ablation and flow. J. Glaciol. 8 (51), 341–352.

Paterson, W.S., 1972. Laurentide ice sheet: Estimated volumes during late Wisconsin. Rev. Geophys. Space Phys. 10 (4), 885–917.

Paterson, W.S.B., 1994. The Physics of Glaciers, third ed. Pergamon, Oxford, England.

Pathare, A.V., Paige, D.A., 2005. The effects of martian orbital variations upon the sublimation and relaxation of north polar troughs and scarps. Icarus 174 (2), 419–443.

Pathare, A.V., Paige, D.A., Turtle, E., 2005. Viscous relaxation of craters within the martian south polar layered deposits. Icarus 174 (2), 396–418.

Phillips, R.J. et al., 2008. Mars north polar deposits: Stratigraphy, age, and geodynamical response. Science 320 (5880), 1182–1185.

Phillips, R.J. et al., 2011. Massive CO_2 ice deposits sequestered in the South Polar Layered Deposits of Mars. Science 332, 838–841.

Plaut, J.J., Kahn, R., Guinness, E.A., Arvidson, R.E., 1988. Accumulation of sedimentary debris in the south polar-region of Mars and implications for climate history. Icarus 76 (2), 357–377.
Plaut, J.J. et al., 2009. Radar evidence for ice in Lobate Debris Aprons in the mid-northern latitudes of Mars. Geophys. Res. Lett. 36. http://dx.doi.org/10.1029/2008GL036379.
Samyn, D., Fitzsimons, S.J., Lorrain, R.D., 2005. Strain-induced phase changes within cold basal ice from Taylor Glacier, Antarctica, indicated by textural and gas analyses. J. Glaciol. 51 (175), 611–619.
Schorghofer, N., 2008. Temperature response of mars to Milankovitch cycles. Geophys. Res. Lett. 35 (18). http://dx.doi.org/10.1029/2008GL034954.
Shean, D.E., 2010. Candidate ice-rich material within equatorial craters on Mars. Geophys. Res. Lett. 37. http://dx.doi.org/10.1029/2010GL045181.
Shean, D.E., Head, J.W., Marchant, D.R., 2005. Origin and evolution of a cold-based tropical mountain glacier on Mars: The Pavonis Mons fan-shaped deposit. J. Geophys. Res. 110. http://dx.doi.org/10.1029/2004JE002360.
Skorov, Yu.V., Markiewics, W.J., Basilevsky, A.T., Keller, H.U., 2001. Stability of water ice under a porous nonvolatile layer: Implications to the south polar layered deposits of Mars. Planet. Space Sci. 49, 59–63.
Smith, P.H. et al., 2009. H_2O at the Phoenix landing site. Science 325, 58–61.
Tanaka, K.L., Rodriguez, J.A.P., Skinner, J.A., Bourke, M.C., Fortezzo, C.M., Herkenhoff, K.E., Kolb, E.J., Okubo, C.H., 2008. North polar region of Mars: Advances in stratigraphy, structure, and erosional modification. Icarus 196 (2), 318–358.
Vasavada, A.R. et al., 2000. Surface properties of Mars' polar layered deposits and polar landing sites. J. Geophys. Res. – Planets 105 (E3), 6961–6969.
Vaughan, D.G., Corr, H.F.J., Doake, C.S.M., Waddington, E.D., 1999. Distortion of isochronous layers in ice revealed by ground-penetrating radar. Nature 398, 323–326.
Waddington, E.D., Neumann, T.A., Koutnik, M.R., Marshall, H.-P., Morse, D.L., 2007. Inference of accumulation-rate patterns from deep layers in glaciers and ice sheets. J. Glaciol. 53 (183), 694–712.
Winebrenner, D.P., Koutnik, M.R., Waddington, E.D., Pathare, A.V., Murray, B.C., Byrne, S., Bamber, J.L., 2008. Evidence for ice flow prior to trough formation in the martian North Polar Layered Deposits. Icarus 195 (1), 90–105.
Winebrenner, D.P., Waddington, E.D., Pathare, A. 2011. Evolution of stratigraphy under the action of ice flow in Gemina Lingula. American Geophysical Union P21D-06 (abstract).
Winebrenner, D.P., Pathare, A., Waddington, E.D., Koutnik, M.R., 2012. Flow modeling of Gemina Lingula with slope-dependent ablation reproduces near-surface radar stratigraphy. American Geophysical Union (abstract).
Zuber, M.T. et al., 1998. Observations of the north polar region of Mars from the Mars Orbiter Laser Altimeter. Science 282, 2053–2060.
Zuber, M.T. et al., 2000. Thermal evolution of Mars from Mars global surveyor topography and gravity. Science 287, 1788–1793.
Zwally, H.J. et al., 2000. Morphology of Mars north polar ice cap. Mars, Polar Science 4112 (abstract).